2

# Atmospheric Turbulence Characterization and Wavefront Sensing by Means of the Moiré Deflectometry

Saifollah Rasouli
*Department of Physics, Institute for Advanced Studies in Basic Sciences (IASBS), Zanjan*
*Optics Research Center, Institute for Advanced Studies in Basic Sciences (IASBS), Zanjan*
*Iran*

## 1. Introduction

When a light beam propagates through the turbulent atmosphere, the wavefront of the beam is distorted, which affect the image quality of ground based telescopes. Adaptive optics is a means for real time compensation of the wavefront distortions. In an adaptive optics system, wavefront distortions are measured by a wavefront sensor, and then using an active optical element such as a deformable mirror the instantaneous wavefront distortions are corrected. On the other hand, three physical effects are observed when a light beam propagates through a turbulent atmosphere: optical scintillation, beam wandering, and fluctuations in the angle-of-arrival (AA). These effects are used for measuring turbulence characteristic parameters. Fluctuations of light propagation direction, referred to as the fluctuations of AA, are measured by various methods. In wavefront sensing applications the AA fluctuations measurement is a basic step.

Various wavefront sensing techniques have been developed for use in a variety of applications ranging from measuring the wave aberrations of human eyes (Lombardo & Lombardo, 2009) to adaptive optics in astronomy (Roddier, 1999). The most commonly used wavefront sensors are the Shack-Hartmann (Platt & Shack, 2001; Shack & Platt, 1971), curvature sensing (Roddier , 1988), shearing interferometry (Leibbrandt et al., 1996), phase retrieval methods (Gonsalves, 1996) and Pyramid wavefront sensor (Ragazzoni & Farinato, 1999). The Shack-Hartmann (SH) sensor is also the most commonly used technique for measurement of turbulence-induced phase distortions for various applications in atmospheric studies and adaptive optics. But, the dynamic range of the SH sensor is limited by the optical parameters of its microlenses, namely, the spacing and the focal length of the microlens array.

In recent years, some novel methods, based on moiré technique, for the study of atmospheric turbulence have been introduced (Rasouli & Tavassoly, 2006b; 2008; Rasouli, 2010). As a result of these works, due to the magnification of the telescope, the use of moiré technique, and the Talbot effect, measurements of fluctuations in the AA can be up to 2 orders of magnitude more precise than other methods. Also, moiré deflectometry have been used to wavefront sensing in various schemes (Rasouli et al., 2009; 2010). In the recent scheme,

an adjustable, high-sensitivity, wide dynamic range two channel wavefront sensor was suggested for measuring distortions of light wavefront transmitted through the atmosphere (Rasouli et al., 2010). In this sensor, a slightly divergent laser beam is passed through the turbulent ground level atmosphere and then a beam-splitter divides it into two beams. The beams pass through a pair of moiré deflectometers which are installed parallel and close together. From deviations in the moiré fringes, two orthogonal components of AA at each location across the wavefront are calculated. The deviations have been deduced in successive frames which allows evolution of the wavefront shape to be determined. In this wavefront sensor the dynamic range and sensitivity of detection are adjustable in a very simple manner. This sensor is more reliable, quite simple, and has many practical applications ranging from wave aberrations of human eyes to adaptive optics in astronomy. Some of the applications, such as measurement of wave aberrations induced by lenses and study of nonlinear optical media, are in progress, now by the author.

At the beginning of the this chapter, moiré pattern, Talbot effect, Talbot interferometry and moiré deflectometry will be briefly reviewed. Also, definition, history and some applications of the moiré technique will be presented. Then, all of the moiré based methods for the atmospheric turbulence study will be reviewed. One of the mean purposes of this chapter is to describe the abilities of the moiré based techniques in the study of atmospheric turbulence with their potentials and limitations. Also, in this chapter a new moiré based wavefront sensing technique that can be used for adaptive optics will be presented. At the end of this chapter, a brief comparison of use of two wavefront sensors, the SH sensor and the two channel moiré deflectometry based wavefront sensor, will be presented.

In addition, a new computationally algorithm for analyzing the moiré fringes will be presented. In this chapter, for the first time, the details of an improved algorithm for processing moiré fringes by means of virtual traces will be presented. By means of the virtual traces one can increase the precision of measurements in all of the moiré based methods, by increasing the moiré fringes spacing, meanwhile at the same time by using a number of virtual traces, the desired spatial resolution is achievable. As a result, the sensitivity of detection is adjustable by merely changing the separation of the gratings and the angle between the rulings of the gratings in moiré deflectometer, and at the same time, the desired spatial resolution is achieved by means of the virtual traces.

## 2. Moiré technique; definition, history and applications

Generally, superposition of two or more periodic or quasi-periodic structures (such as screens, grids or gratings) leads to a coarser structure, named moiré pattern or moiré fringes. The moiré phenomenon has been known for a long time; it was already used by the Chinese in ancient times for creating an effect of dynamic patterns in silk cloth. However, modern scientific research into the moiré technique and its application started only in the second half of the 19th century. The word moiré seems to be used for the first time in scientific literature by Mulot (Patorski & Kujawinska, 1993).

The moiré technique has been applied widely in different fields of science and engineering, such as metrology and optical testing. It is used to study numerous static physical phenomena such as refractive index gradient (Karny & Kafri, 1982; Ranjbar et al., 2006). In addition, it has a severe potential to study dynamical phenomena such as atmospheric turbulence (Rasouli & Tavassoly, 2006a;b; 2008; Rasouli, 2010), vibrations (Harding & Harris, 1983), nonlinear refractive index measurements (Jamshidi-Ghaleh & Mansour, 2004; Rasouli et al., 2011), displacements and stress (Post et al., 1993; Walker, 2004), velocity measurement

(Tay et al., 2004), acceleration sensing (Oberthaler et al., 1996), etc. The moiré pattern can be created, for example, when two similar grids (or gratings) are overlaid at a small angle, or when they have slightly different mesh sizes. In many applications one of the superposed gratings is the image of a physical grating (Rasouli & Tavassoly, 2005; Ranjbar et al., 2006; Rasouli & Tavassoly, 2006a). When the image forming lights propagate in a perturbed medium, the image grating is distorted and the distortion is magnified by the moiré pattern.

Briefly, moiré technique has diverse applications in the measurements of displacement and light deflection, and it improves the precision of the measurements remarkably. Besides, the required instrumentation is usually simple and inexpensive.

## 3. Moiré pattern, Talbot effect, Talbot interferometry and moiré deflectometry

As it mentioned, moiré pattern can be created, when two similar straight-line grids (or gratings) are superimposed at a small angle, Fig. 1, or when they have slightly different mesh sizes, Fig. 2. In many applications one of the superimposed gratings is the image of a physical grating or is one of the self-images of the first grating. In applications, the former case is named projection moiré technique and the latter case is called moiré deflectometry or Talbot interferometry.

When a grating is illuminated with a spatially coherent light source, exact images and many other images can be found at finite distances from the grating. This self-imaging phenomenon is named the Talbot effect. By superimposing another grating on one of the self-images of the first grating, moiré fringes are formed. The Talbot interferometry and the moiré deflectometry are not identical, although they seem quite similar at a first glance. In the Talbot interferometry setup, a collimated light beam passes through a grating and then through a distorting phase object. The distorted shadow of the grating forms a moiré pattern with a second grating located at a Talbot plane (also known as Fourier plane). The moiré deflectometry measures ray deflections in the paraxial approximation, provided that the phase object (or the specular object) is placed in front of the two gratings. The resulting fringe pattern, is a map of ray deflections corresponding to the optical properties of the inspected object. Generally, when the image forming lights propagate in a perturbed medium the image grating is distorted and the distortion is magnified by moiré pattern. When the similar gratings are overlaid at a small angle, the moiré magnification is given by (Rasouli & Tavassoly, 2006b)

$$\frac{d_m}{d} = \frac{1}{2sin(\theta/2)} \simeq \frac{1}{\theta}\,, \tag{1}$$

where $d_m$, $d$, and $\theta$ stand for moiré fringe spacing, the pitch of the gratings, and gratings' angle.

In case of parallel moiré pattern (Rasouli & Tavassoly, 2008; Rasouli et al., 2011), when the gratings vectors are parallel together and the resulting moiré fringes are parallel to the gratings lines, the moiré magnification is given by

$$\frac{d_m}{d} = \frac{d}{\delta d}\,, \tag{2}$$

where $\delta d$ stands for the difference of mesh sizes of the gratings.

Generally, in the moiré technique displacing one of the gratings by $l$ in a direction normal to its rulings leads to a moiré fringe shift $s$, given by (Rasouli & Tavassoly, 2006b)

$$s = \frac{d}{d_m}\, l. \tag{3}$$

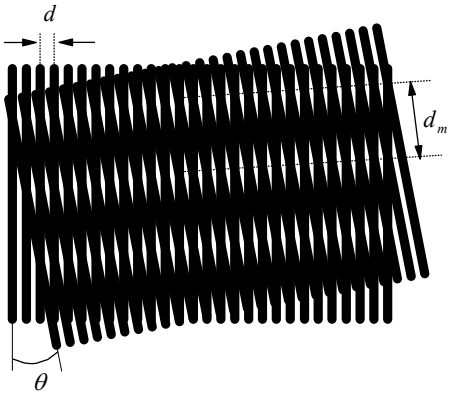


Fig. 1. A moiré pattern, formed by superimposing two sets of parallel lines, one set rotated by angle $\theta$ with respect to the other (Rasouli & Tavassoly, 2007).

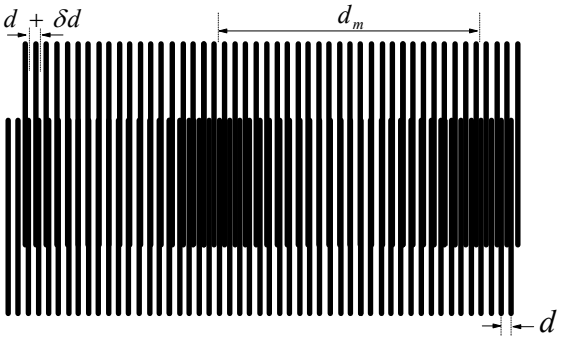


Fig. 2. A moiré pattern, formed by superimposing two sets of parallel lines, when they have slightly different mesh sizes (Rasouli, 2007).

## 4. Measuring atmospheric turbulence parameters by means of the moiré technique

Changes in ground surface temperature create turbulence in the atmosphere. Optical turbulence is defined as the fluctuations in the index of refraction resulting from small temperature fluctuations. Three physical effects are observed when a light beam propagates through a turbulent atmosphere: optical scintillation, beam wandering, and fluctuations in the AA. These effects are used for measuring turbulence characteristic parameters. Fluctuations

of light propagation direction, referred to as the fluctuations of AA, are measured by various methods. In astronomical applications the AA fluctuations measurement is a basic step. Differential image motion monitor (Sarazin, 1990) and generalized seeing monitor systems (Ziad et al., 2000) are based on AA fluctuations. The edge image waviness effect (Belen'kii et al., 2001) is also based on AA fluctuations. In some conventional methods the fluctuations of AA are derived from the displacements of one or two image points on the image of a distant object in a telescope. In other techniques the displacements of the image of an edge are exploited. The precisions of these techniques are limited to the pixel size of the recoding CCD. In following we review some simple but elegant methods that have been presented recently in measuring the AA fluctuations and the related atmospheric turbulence parameters by means of moiré technique.

### 4.1 Incoherent imaging of a grating in turbulent atmosphere by a telescope

The starting work of the study of atmospheric turbulence by means of moiré technique was published in Rasouli & Tavassoly (2006a). In this work moiré technique have been used in measuring the refractive index structure constant, $C_n^2$, and its profile in the ground level atmosphere. In this method from a low frequency sinusoidal amplitude grating, installed at certain distance from a telescope, successive images are recorded and stored in a computer. By superimposing the recorded images on one of the images, the moiré patterns are formed. Also, this technique have been used in measuring the modulation transfer functions of the ground-level atmosphere (Rasouli et al., 2006). In the present approach after the filed process, by superimposing the images of the grating the moiré patterns are formed. Thus, observation of the AA fluctuations visually improved by the moiré magnification, but it was not increased precision of the AA fluctuations measurement. Also, this method is not a real-time technique. But, compared to the conventional methods (Belen'kii et al., 2001; Sarazin, 1990; Ziad et al., 2000) in this configuration across a rather large cross section of the atmosphere one can access to large volume of 2-D data.

In this method, when an image point on the focal plane of a telescope objective is displaced by $l$ the AA changes by

$$\alpha = l/f, \tag{4}$$

where $f$ is the objective focal length. Thus, order of measurement precision of the method is similar to the order of measurement precision of the conventional methods like differential image motion monitor (DIMM) (Belen'kii et al., 2001; Sarazin, 1990). Meanwhile, in this method a grating on full size of a CCD's screen are being imaged, but for example in the differential image motion monitor two image points are formed on small section of a CCD's screen.

### 4.2 Incoherent imaging of a grating on another grating in turbulent atmosphere by a telescope

In 2006 a new technique, based on moiré fringe displacement, for measuring the AA fluctuations have been introduced (Rasouli & Tavassoly, 2006b). This technique have two main advantages over the previous methods. The displacement of the image grating lines can be magnified about ten times, and many lines of the image grating provide large volume of data which lead to very reliable result. Besides, access to the displacement data over a rather large area is very useful for the evaluation of the turbulence parameters depending on correlations of displacements. The brief description of the technique implementation is as follows. A low frequency grating is installed at a suitable distance from a telescope. The image

of the grating, practically forms at the focal plane of the telescope objective. Superimposing a physical grating of the same pitch as the image grating onto the latter forms the moiré pattern. Recording the consecutive moiré patterns with a CCD camera connected to a computer and monitoring the traces of the moiré fringes in each pattern yields the AA fluctuations versus time across the grating image. A schematic diagram of the experimental setup is shown in Fig. 3.

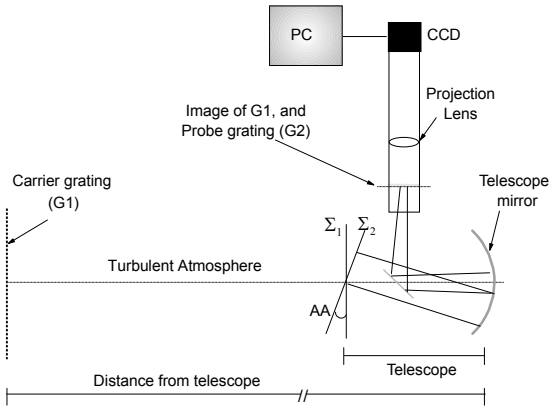


Fig. 3. Schematic diagram of the instrument used for atmosphere turbulence study by projection moiré technique, incoherent imaging of a grating on another grating in turbulent atmosphere by a telescope. (Rasouli & Tavassoly, 2006b; 2007).

The typical real time moiré fringes obtained by the set-up is shown in Fig. 4(a), and its corresponding low frequency illumination after a spatial fast Fourier transform method to low pass filter the data is shown in Fig. 4(b).

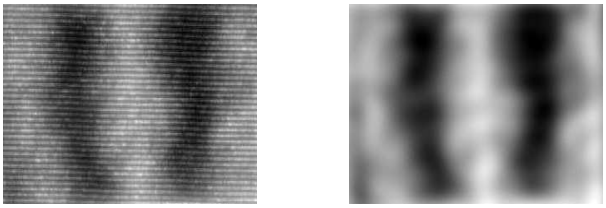

(a) (b)

Fig. 4. (a) Typical moiré pattern recorded by the set-up in Fig. 3, (b) the corresponding low frequency illumination (Rasouli & Tavassoly, 2007).

In this method, the component $\alpha$ of the AA fluctuation in the direction perpendicular to the lines of the carrier grating (parallel to the moiré fringes) is given by (Rasouli & Tavassoly, 2006b)

$$\alpha = \frac{1}{f}\frac{d}{d_m}\, s, \tag{5}$$

where $f$, $d$, $d_m$, and $s$ are the telescope focal length, the pitch of the probe gratings, the moiré fringes spacing, and the moiré fringe displacement, respectively. Compared to Eq. (4), here an improving factor $\frac{d}{d_m}$ appears. When the angle between the lines of superimposed gratings

is less than $6^o$, the magnification is more than ten times. In other word: *"Light-beam deflections due to atmospheric turbulence are one order of magnitude more precise with the aid of moiré patterns (Rasouli & Tavassoly, 2007)."*

### 4.3 Application of moiré deflectometry in atmospheric turbulence measurements

The next scheme, noteworthy both for its simplicity and its cleverness, illustrates the basic idea (ICO Newsletter, April 2009; Rasouli & Tavassoly, 2008). A monochromatic light wave from a small and distant source is incident on a fine pitch Ronchi ruling. A short distance beyond, a Talbot image of the ruling appears.

With diverging-light illumination of the Ronchi ruling, the Talbot image is slightly larger in scale than the ruling itself. If a duplicate of the ruling is placed in the Talbot image plane, in exactly the same orientation as the original ruling, large fringes result from the moiré effect.

Most importantly, any turbulence-produced local variations in the AA of the incident wave, even if quite small, manifest themselves as easily seen distortions of the moiré fringe pattern. These distortions, captured by a CCD video camera, are analysed by a computer program. The technique have been used to determine parameters that characterize the strength of turbulence measured along horizontal paths. A schematic diagram of the experimental setup is shown in Fig. 5.

In this method the component $\alpha$ of the AA fluctuation in the direction perpendicular to the lines of the gratings is given by (Rasouli & Tavassoly, 2008)

$$\alpha = \frac{d}{d_m}\frac{s}{Z_k}, \tag{6}$$

where $Z_k$ denotes the $k$th self-image or Talbot's distance is given by (Patorski & Kujawinska, 1993)

$$2k\frac{d^2}{\lambda} = \frac{LZ_k}{L+Z_k}, \tag{7}$$

where $\lambda$ is the light wavelength and $L$ is the distance between $G1$ and the source.

The implementation of the technique is straightforward, a telescope is not required, fluctuations can be magnified more than ten times, and the precision of the technique can be similar to that reported in the previous work (Rasouli & Tavassoly, 2006b).

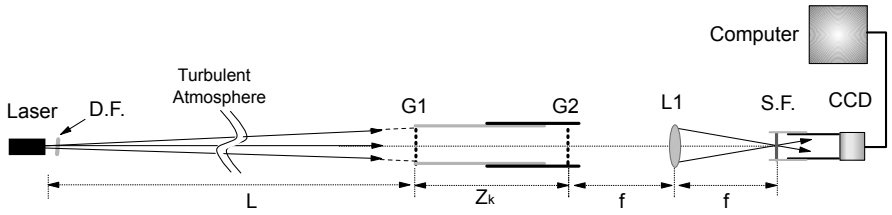


Fig. 5. Schematic diagram of the application of moiré deflectometry in atmospheric turbulence measurements. *D.F.*, *G*1, *G*2, *L*1, and *S.F.*, stand for the neutral density filter, first grating, second grating, Fourier transforming lens, and the spatial filter, respectively (Rasouli & Tavassoly, 2008).

### 4.4 Use of a moiré deflectometer on a telescope for atmospheric turbulence measurements

Recently, a highly sensitive and high spatial resolution instrument for the study of atmospheric turbulence by measuring the fluctuation of the AA on the telescope aperture plane have been constructed (Rasouli, 2010). A schematic diagram of the instrument is shown in Fig. 6. A slightly divergent laser beam passes through a turbulent ground level atmosphere and enters the telescope aperture. The laser beam is recollimated behind the telescope's focal point by means of a collimator. The collimated beam passes through a moiré deflectometer. Compared to the previous moiré based methods, because of the large area of the telescope aperture, this instrument is more suitable for studying spatial and temporal properties of wavefronts. Because of the magnifications of the telescope and moiré deflectometry, the precision of measurement of the technique is one order of magnitude more precise than previous methods. In other word, the precision of AA fluctuations measurement for the second time have been improved. This instrument has a very good potential for wavefront sensing and adaptive optics applications in astronomy with more sensitivity. Besides, a modified version of this instrument can be used to study other turbulent media such as special fluids and gases. Also, this method is a reliable way to investigate turbulence models experimentally.

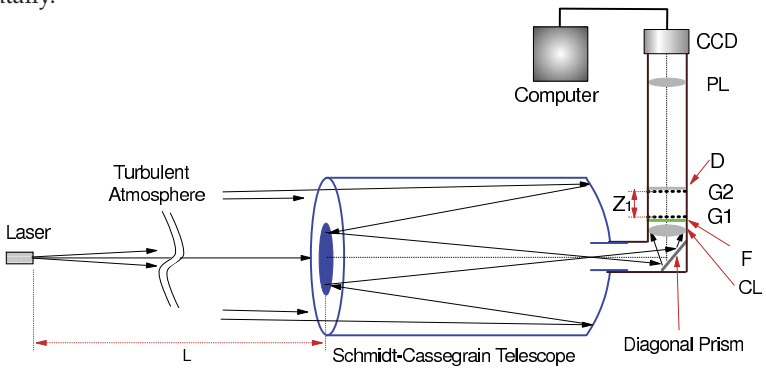


Fig. 6. Schematic diagram of the instrument; use of a moiré deflectometer on a telescope. $CL$, $F$, $G1$, $G2$, and $PL$, stand for the collimating lens, bandpass filter, first grating, second grating, and the lens that projects the moiré pattern produced on the diffuser D on the CCD, respectively. (Rasouli, 2010).

Here, the component $\alpha$ of the AA fluctuation on the telescope aperture plane is given by(Rasouli, 2010):

$$\alpha = \frac{f'}{f}\frac{1}{Z_k}\frac{d}{d_m}s, \tag{8}$$

where $f$ is the telescope focal length and $f'$ is the focal length of the collimating lens. Compared to Eq. (6) here an improving factor $f'/f$ appears. For example, in the work of Rasouli (2010), $f$=200 cm and $f' = 13.5$ cm have been used, thus the magnification is more than ten times. In other word, the precision of AA fluctuations measurement for second time in this work have been improved. *As a result, due to the magnification of the telescope, the use of Moiré technique, and the Talbot effect, measurements of fluctuations in the AA can be up to 2 orders of magnitude more precise than other methods* (Rasouli & Tavassoly, 2006b; 2008; Rasouli, 2010).

| Method | $\alpha_{min}$ | Volume of data | Processing way |
|---|---|---|---|
| DIMM | order of one arc sec | Two image points | Real-time |
| IIGT | 0.5 arc sec | are equal to the CCD pixels number | Non real-time |
| IIGGT | 0.06 arc sec | are equal to the CCD pixels number | Real-time |
| MD | 0.27 arc sec | are equal to the CCD pixels number | Real-time |
| MDT | 0.01 arc sec | are equal to the CCD pixels number | Real-time |

Table 1. Comparison of sensitivities and spatial resolutions of different methods; DIMM, IIGT, IIGGT, MD, MDT are stand for the differential image motion monitor, incoherent imaging of a grating by a telescope, incoherent imaging of a grating on another grating by a telescope, moiré deflectometry method, use of a moiré deflectometer on a telescope, respectively. $\alpha_{min}$ stands for the minimum measurable AA fluctuation.

### 4.5 Comparison of sensitivities and spatial resolutions of different moiré based methods

According to Eqs. (5), (6), and (8), in all of the moiré based methods by increasing the gratings distance, decreasing the pitch of the gratings, or increasing the moiré fringes spacing, the measurement precision is improved. Let us now to compare the sensitivities of all of the reviewed methods by considering typical values that can be used in the works namely: $l = 5\ \mu m$, $d$=1/15 mm, $f$=2 m, $f'$=10 cm, $Z_k$ =0.5 m, $s/d_m$= 1/100, the minimum measurable AA fluctuations are obtained using Eqs. (4)-(6), and (8); $2.5 \times 10^{-6}$, $3.3 \times 10^{-7}$, $1.3 \times 10^{-6}$, and $6.6 \times 10^{-8}$ rad, respectively. More details of the different methods are presented in Table 1.

In comparing implementation of different methods, the implementation of the incoherent imaging of a grating by a telescope is not straightforward. Implementation of the moiré deflectometry method and use of a moiré deflectometer on a telescope are very straightforward. Also, the last method, because of its measurement precision and large area of the telescope aperture has potential applications in diverse fields.

### 4.6 A brief summary on the study of atmospheric turbulence by means of moiré technique

In brief incorporation of moiré technique in the study of atmospheric turbulence provides the following advantages:
- Access to large volume of data in 2-Ds
- Correlations calculations in 2-Ds at desired scale
- The required instrumentation is usually simple and inexpensive
- The presented techniques usually are very flexible and can be applied in a wide range of turbulence strengths, by choosing gratings of adequate pitch, size, and separation.
- Improvement of measurement precision; as a result of the works, measurements of fluctuations in the AA can be up to 2 orders of magnitude more precise than other methods.

## 5. Wavefront sensing based on moiré deflectometry

Recently, a wide dynamic range two channel wavefront sensor based on moiré deflectometry has been constructed for measuring atmospheric distortions of wavefront (Rasouli et al., 2009; 2010). Schematic diagram of the sensor is shown in Fig. 7. In this sensor, a collimated laser beam passes through a time-varying refractive index field, like a turbulent medium, and then a beam-splitter divides it into two beams. A mirror reflects the second beam into a direction parallel to the first beam propagation direction, and the beams pass through a pair of moiré deflectometers. The moiré deflectometers are installed parallel and close together. The gratings' rulings are roughly parallel in each moiré deflectometer but are perpendicular

in the two beams. Moiré patterns are formed on a plane where the second gratings of the moiré deflectometers and a diffuser are installed. The moiré patterns are projected on a CCD camera. Using moiré fringes fluctuations two orthogonal components of the AA across the wavefront have been calculated. The fluctuations have been deduced in successive frames, and then evolution of the wavefront shape is determined. The dynamic range and sensitivity of detection are adjustable by merely changing the distance between two gratings in both moiré deflectometers and relative grating ruling orientation. The spatial resolution of the method is also adjustable by means of bright, dark, and virtual traces for given moiré fringes without paying a toll in the measurement precision. The implementation of the technique is straightforward. The measurement is relatively insensitive to the alignment of the beam into the sensor. This sensor has many practical applications ranging from wave aberrations of human eyes to adaptive optics in astronomy.

In this sensor, the incident wavefront gradients in $x$ and $y$-directions at a point $(x, y)$ are determined by (Rasouli et al., 2010)

$$\left[\frac{\partial U(x,y)}{\partial x}, \frac{\partial U(x,y)}{\partial y}\right] = \frac{d}{Z_k}\left[\frac{s_y}{d_m^{'}}, \frac{s_x}{d_m}\right]. \tag{9}$$

where, $d_m$, $d_m^{'}$, $s_y$, and $s_x$ are the moiré fringe spacing in the first and second channels, and the moiré fringes shifts in the first and second channels, respectively.

Typical reconstructed wavefront surface for a collimated laser beam passes through a turbulent column of hot water vapor rising from a small cup using this wavefront sensor in a region of $20mm \times 20mm$ are shown in Fig. 8.

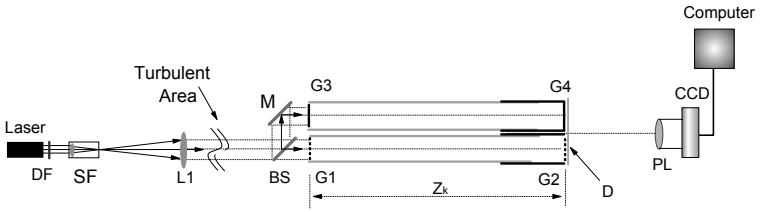


Fig. 7. Schematic diagram of the experimental setup of two channel wavefront sensor. $G$, $L$, $M$, and $S.F.$ stand for the gratings, lenses, mirrors, and spatial filters respectively. $D.F.$, $B.S.$ and $Z_k$ stand for the neutral density filter, beam splitter, and talbot distance, respectively.

### 5.1 An improved algorithm for processing moiré fringes by means of virtual traces

The most commonly approach in the moiré fringes processing are based on measurement of the displacements of the bright or dark moiré fringes. In this approach, according to the Eqs. (3), (5), (6), (8) and (9), by increasing the moiré fringe spacing the precision of measurements can be improved. But, then the number of moiré fringes in the field of view is decreased and the spatial resolution of the method is decreased. Recently, an improved algorithm have been used for processing the moiré fringes to overcome this limitation (Rasouli et al., 2010; Rasouli & Dashti, 2011). A new concept that is called virtual traces in the moiré patterns have been introduced . In this approach, the traces of bright moiré fringes, dark moiré fringes, and of points with intensities equal to the mean intensity of the adjacent bright and dark traces (first order virtual traces) were determined. One can potentially produce a large number of virtual traces between two adjacent bright and dark traces by using their intensities and

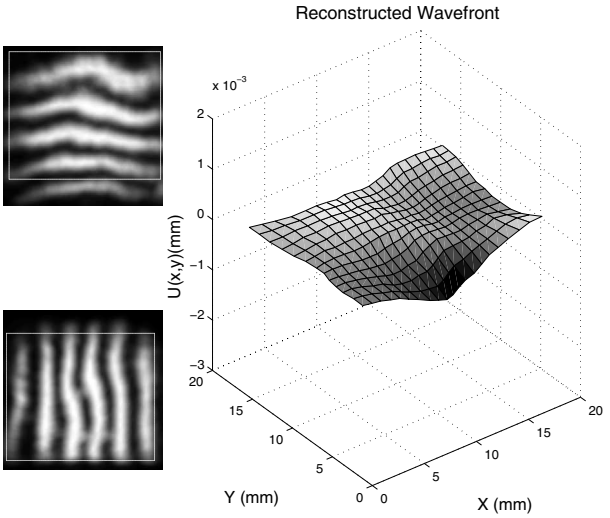


Fig. 8. Moiré fringes in the horizontal and vertical directions and the reconstructed wavefront, surface plot, corresponding to distortions generated by a turbulent column of hot water vapor rising from a small cup in a region of $20 \times 20$ mm$^2$.

locations. One can increase the precision of measurements by increasing the moiré fringes spacing, meanwhile at the same time by using a number of virtual traces, the desired spatial resolution is achievable. Thus, the sensitivity of detection is adjustable by merely changing the separation of the gratings and the angle between the rulings of the gratings in moiré deflectometer, and at the same time, the desired spatial resolution is achieved by means of the virtual traces.

Here, for the first time, the details of the mentioned improved algorithm for processing moiré fringes by means of virtual traces are presented. We use the algorithm on one of the moiré fringes of Fig. 8. As it previously mentioned, the distortions on the fringes correspond to a turbulent column of hot water vapor rising from a small cup. Low-frequency illumination distribution of the first bright and dark moiré fringes in the horizontal direction are shown in Fig. 9. The corresponding derived bright ($I_b$) and dark ($I_d$) traces are shown in Fig. 10.

Mathematically, the moiré fringes intensity profile in direction perpendicular to the moiré fringes, after a spatial fast Fourier transform method to low pass filter the data, can be written as

$$I(y) = \left[ (\frac{I_b + I_d}{2}) + (\frac{I_b - I_d}{2}) cos \frac{2\pi}{d_m}(y + y_{0b}) \right], \tag{10}$$

where $d_m$, $I_b$, $I_d$, and $y_{0b}$ are the moiré fringes spacing, the intensity of bright and dark traces, and the position of the reference bright trace, respectively. Here, we have used $d_m$ instead of previously used $d_m^{'}$.

It should be mentioned that, due to the presence of air turbulence in the path, the image grating - one of the superimposed gratings for generation the moiré pattern - is distorted and the distortion is magnified by the moiré pattern. As a result, the moiré fringes intensity profile a little differs from Eq. (10). We will show the distorted moiré fringes intensity profile by $I'(y)$.

From Eq. (10), mid points between the adjacent bright and dark traces have an intensity equal to $\frac{I_b+I_d}{2}$. Now, for the case of distorted moiré pattern, the traces of points with intensities equal to the mean intensity of the adjacent bright and dark traces ($I_{vir}^{(1)} = \frac{I'_b+I'_d}{2}$) to be determined the first order virtual trace. By use of following equation in all of the columns of the intensity distribution of the moiré pattern, one can find the first order virtual trace

$$I_{vir}^{(1)} = \frac{I'_b + I'_d}{2} = I'(y_{vir}^{(1)}) \rightarrow y_{vir}^{(1)} = y\left(I' = \frac{I'_b + I'_d}{2}\right). \tag{11}$$

Intensity profile of moiré fringes in the direction perpendicular to the moiré fringes and the corresponding point on the first order virtual trace, $(y_{vir}^{(1)}, I_{vir}^{(1)})$, are shown in Fig. 11.

One can potentially produce a large number of virtual traces between two adjacent bright and dark traces by using their intensities and locations. In the non-distorted moiré pattern, by finding the intensity of the mid points between the first order virtual trace and the adjacent bright and dark traces using Eq. (10), one can produce two second order virtual traces, that are named $I_{vir}^{(2b)}$ and $I_{vir}^{(2d)}$, respectively. For non-distorted moiré pattern, their intensities are given by

$$I_{vir}^{(2b)} = \left[(\frac{I_b + I_d}{2}) + (\frac{I_b - I_d}{2})cos\frac{2\pi}{d_m}(y_{vir}^{(2b)} + y_{0b})\right], \tag{12}$$

$$I_{vir}^{(2d)} = \left[(\frac{I_b + I_d}{2}) + (\frac{I_b - I_d}{2})cos\frac{2\pi}{d_m}(y_{vir}^{(2d)} + y_{0b})\right], \tag{13}$$

where, $y_{vir}^{(2b)} = \frac{y_b+y_{vir}^{(1)}}{2}$ and $y_{vir}^{(2b)} = \frac{y_d+y_{vir}^{(1)}}{2}$. Now, for the case of distorted moiré pattern, the traces of points with intensities equal to the intensity of points with $y = \frac{y_b+y_{vir}^{(1)}}{2}$ and $y = \frac{y_d+y_{vir}^{(1)}}{2}$, were obtained from Eqs. (12) and (13), to be determined the second order virtual traces, $I_{vir}^{(2b)}$ and $I_{vir}^{(2b)}$, respectively. By use of following equations in all of the columns of the intensity distribution of moiré pattern, one can find the second order virtual traces

$$I_{vir}^{(2b)} = I'\left(y = \frac{y_b + y_{vir}^{(1)}}{2}\right) \rightarrow y_{vir}^{(2b)} = y\left(I_{vir}^{(2b)}\right), \tag{14}$$

$$I_{vir}^{(2d)} = I'\left(y = \frac{y_d + y_{vir}^{(1)}}{2}\right) \rightarrow y_{vir}^{(2d)} = y\left(I_{vir}^{(2d)}\right). \tag{15}$$

The procedure to produce higher order virtual traces is similar to that one were used for the second order virtual traces. In Fig. 12, three virtual traces, $I_{vir}^{(1)}$, $I_{vir}^{(2b)}$, and $I_{vir}^{(2d)}$ are produced between two adjacent bright and dark traces by using their intensities and locations.

### 5.2 Wavefront reconstruction

Another major part of a wavefront sensor is a software to convert the 2-D wavefront gradients data into 2-D wavefront phase data. In order to perform the wavefront reconstruction from

Fig. 9. Low-frequency illumination distribution of a typical bright and dark moiré fringes.

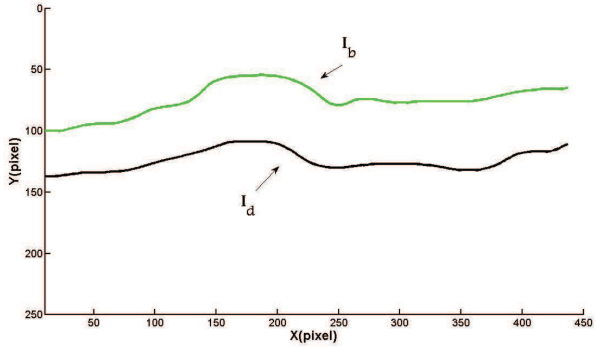


Fig. 10. The derived traces of bright ($I_b$) and dark ($I_d$) moiré fringes corresponding to the fringes are shown in Fig. 9.

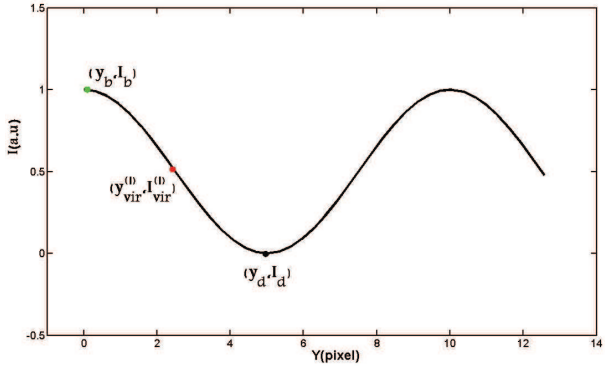


Fig. 11. Typical intensity profile of non-distorted moiré fringes in the direction perpendicular to the moiré fringes and the corresponding point on the first order virtual trace.

the measured moiré patterns, we consider the displacements of the bright, dark, and the first order virtual traces with respect to their reference positions, which represents an estimate of the local $x$-gradients or $y$-gradients of the wavefront phase. The reference positions of the traces are determined from a long-exposure frame. In practice, by considering two sets of vertical and horizontal moiré traces of a frame in a $x$-$y$ coordinate system (the vertical and horizontal traces are overlapped in the $x$-$y$ coordinate system), the intersection points of the vertical and horizontal bright, dark, and the first order virtual traces are determined. $x$-gradients and $y$-gradients of the wavefront are deduced from the displacements of the intersection points in successive frames. From this 2-D gradient field we performed an estimate of the wavefront.

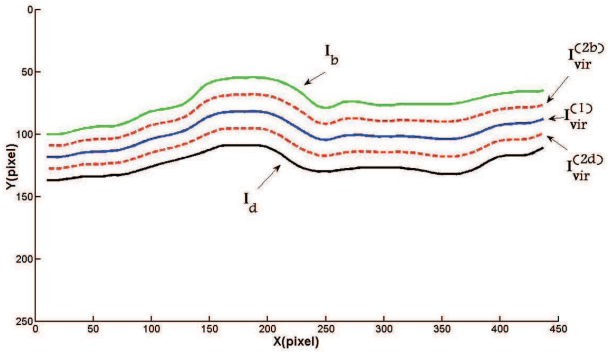


Fig. 12. Three virtual traces are produced between two adjacent bright and dark traces by using their intensities and locations.

Algorithmically, this involves the calculation of a surface by an integration-like process. The reconstruction problem can be expressed in a matrix-algebra framework. The unknowns, a vector $\Phi$ of N phase values over a grid, must be calculated from the data, from a measurement vector $\mathbf{S}$ of $M$ elements of wavefront gradients in two directions. In the context of wavefront reconstruction, a general linear relation like $\Phi = \mathbf{BS}$ is used, where $\mathbf{B}$ is the so-called reconstruction matrix (Roddier, 1999). A number of techniques are available to derive reconstruction matrix (Fried, 1977; Herrmann, 1980; Hunt, 1979; Southwell, 1980). A linear model of wavefront sensor allows the linking of the measurements $\mathbf{S}$ to the incoming wavefront or its phase. The matrix equation between $\mathbf{S}$ and $\Phi$ reads as $\mathbf{S} = \mathbf{A}\Phi$, where $\mathbf{A}$ is called the interaction matrix. For the geometry of discretization, the 2-D map of intersection points of the traces, the interaction matrix is determined, then the reconstruction matrix is obtained. In the mentioned work Hudgin's and Frid's discretization have been examined (Herrmann, 1980; Hunt, 1979).

### 5.3 Comparison of SH method and moiré deflectometry based two channel wavefront sensor

In this section, an adjustable, high sensitivity, wide dynamic range two channel wavefront sensor based on moiré deflectometry has been reviewed. In this sensor the dynamic range and sensitivity of detection are adjustable by merely changing the separation of the gratings and the angle between the rulings of the gratings in both the moiré deflectometers. This overcomes the deficiency of the Shack-Hartman sensors in that these require expensive retrofitting to change sensitivity. The spatial resolution of the method is also adjustable by means of bright, dark, and virtual traces for a given set of moiré fringes without paying a toll in the measurement precision. By this method discontinuous steps in the wavefront are detectable, because AA fluctuations are measured across the wavefront. Also, unlike the SH sensor, in this sensor the measurement is relatively insensitive to the alignment of the beam into the sensor. The implementation of the technique is straightforward and it overcomes some of the technical difficulties of the SH technique. The required instrumentation for this sensor is usually simple and inexpensive. This sensor has many practical applications ranging from wave aberrations of human eyes to adaptive optics in astronomy.

Finally, for low light applications as one would normally expect in astronomy (to work with stars), the sensor can be performed with phase gratings on a large-sized telescope in

conjunction by use of a highly sensitive CCD. Also, it seems that using a laser guide star one can overcome to this limitation.

## 6. References

Belen'kii, M. S.; Stewart, J. M. & Gillespie, P. (2001). Turbulence-induced edge image waviness: theory and experiment, *Appl. Opt.*, Vol. 40: 1321–1328.

Fried, D. L. (1977). Least-square fitting a wavefront distortion estimate to an array of phase-difference measurements, *J. Opt. Soc. Am.*, Vol. 67: 370–375.

Gonsalves, R. A. (1982). Phase retrieval and diversity in adaptive optics, *Opt. Eng.*, Vol. 21: 829–832.

Harding, K. G. & Harris, J. S. (1983). Projection moiré interferometer for vibration analysis, *Appl. Opt.*, Vol. 22: 856–861.

Herrmann, J. (1980). Least-squares wavefront errors of minimum norm, *J. Opt. Soc. Am.*, Vol. 70: 28–35.

Hunt, B. R. (1979). Matrix formulation of the reconstruction of phase values from phase differences, *J. Opt. Soc. Am.*, Vol. 69: 393–399.

ICO Newsletter, (2009). *ICO Newsletter*, April 2009, Number 79.

Jamshidi-Ghaleh, K. & Mansour, N. (2004). Nonlinear refraction measurements of materials using the moiré deflectometry, *Optics Communications*, Vol. 234: 419–425.

Karny, Z. & Kafri, O. (1982). Refractive-index measurements by moiré deflectometry, *Appl. Opt.*, Vol. 21(18): 3326–3328.

Leibbrandt, G. W. R.; Harbers, G. & Kunst, P. J. (1996). Wavefront analysis with high accuracy by use of a double-grating lateral shearing interferometer, *Appl. Opt.*, Vol. 35: 6151–6161.

Lombardo, M. & Lombardo, G. (2009). New methods and techniques for sensing the wave aberrations of human eyes, *Clinical and Experimental Optometry*, Vol. 92: 176–186.

Nishijima, Y. & Oster, G. (1983). Moiré patterns: Their application to refractive index gradient measurements, *J. Opt. Soc. Am.*, Vol. 54: 1–5.

Oberthaler, M. K.; Bernet, S.; Rasel, Et. M.; Schmiedmayer, J. & Zeilinger, A. (1996). Inertial sensing with classical atomic beams, *Phys. Rev. A*, Vol. 54(4): 3165–3176.

Patorski, K. & Kujawinska, M. (1993). *Handbook of the moiré fringe technique*, Elsevier, Amsterdam.

Platt, B. C. & Shack, R. V. (2001). History and principles of Shack-Hartmann wavefront sensing, *Journal of Refractive Surgery*, Vol. 17: S573–S577.

Post, D.; Han, B. & Ifju, P. (1993). *High Sensitivity moiré: experimental analysis for mechanics and materials*, Springer, Berlin, Germany.

Ragazzoni, R. & Farinato, J. (1999). Phase retrieval and diversity in adaptive optics, *Opt. Eng.*, Vol. 350: L23–L26.

Rasouli, S. & Tavassoly, M. T. (2005). Moiré deflectometer for measuring distortion in sheet glasses, *Proceedings of SPIE, ICO20: Optical Devices and Instruments*, pp. 6024, doi: 10.1117/12.666818, SPIE.

Ranjbar, S.; Khalesifard, H. R.; & Rasouli, S. (2006). Nondestructive measurement of refractive index profile of optical fiber preforms using moiré technique and phase shift method, *Proceedings of SPIE, ICO20: Optical Communication*, pp. 602520, doi: 10.1117/12.667094, SPIE.

Rasouli, S. & Tavassoly, M. T. (2006). Measurement of the refractive-index structure constant, Cn2, and its profile in the ground level atmosphere by moiré technique, *Proceedings*

*of SPIE, Optics in Atmospheric Propagation and Adaptive Systems IX*, pp. 63640G, doi: 10.1117/12.683873, SPIE.

Rasouli, S.; Madanipour, K. & Tavassoly, M. T. (2006). Measurement of modulation transfer function of the atmosphere in the surface layer by moiré technique, *Proceedings of SPIE, Optics in Atmospheric Propagation and Adaptive Systems IX*, pp. 63640K, doi: 10.1117/12.687614, SPIE.

Rasouli, S. & Tavassoly, M. T. (2006). Application of moiré technique to the measurement of the atmospheric turbulence parameters related to the angle of arrival fluctuations, *Opt. Lett.*, Vol. 31(22): 3276 – 3278, ISSN 0146-9592.

Rasouli, S. & Tavassoly, M. T. (2007). Moiré technique improves the measurement of atmospheric turbulence parameters. *SPIE Newsroom*, DOI 10.1117/2.1200702.0569. http://spie.org/documents/Newsroom/Imported/0569/0569-2007-02-20.pdf.

Rasouli, S. (2007). *Ph. D. Thesis: Study of the atmosphere turbulence parameters and large scale structure vibrations using moiré technique*, IASBS, Zanjan, IRAN.

Rasouli, S. & Tavassoly, M. T. (2008). Application of the moiré deflectometry on divergent laser beam to the measurement of the angle of arrival fluctuations and the refractive index structure constant in the turbulent atmosphere, *Opt. Lett.*, Vol. 33(9): 980 – 982, ISSN 0146-9592

Rasouli, S.; Ramaprakash, A. N.; Das, H. K.; Rajarshi, C. V.; Y. Rajabi; & Dashti, M. (2009). Twochannel wavefront sensor arrangement employing moiré deflectometry, *Proceedings of SPIE, Optics in Atmospheric Propagation and Adaptive Systems XII*, pp. 74760K-1, doi: 10.1117/12.829962, SPIE.

Rasouli, S. (2010). Use of a moiré deflectometer on a telescope for atmospheric turbulence measurements, *Opt. Lett.*, Vol. 35(9): 1470 – 1472, ISSN 0146-9592.

Rasouli, S.; Dashti, M.; & Ramaprakash, A. N. (2010). An adjustable, high-sensitivity, wide dynamic range two channel wavefront sensor based on the moiré deflectometry, *Opt. Exp.*, Vol. 18(23): 23906 – 23915.

Rasouli, S. & Dashti, M. (2010). An improved algorithm for processing moiré fringes by means of virtual traces, *Proceeding of 17th Iranian Conference on Optics and Photonics*, pp. 252-255, 2011, (in Persian).

Rasouli, S.; Ghasemi, H.; Tavassoly, M. T. & Khalesifard, H. R. (2011). Application of "parallel" moiré deflectometry and the single beam Z-scan technique in the measurement of the nonlinear refractive index, *Appl. Opt.*, Vol. 50(16): 2356–2360.

Roddier, E. (1988). Curvature sensing and compensation: a new concept in adaptive optics, *Appl. Opt.*, Vol. 27: 1223–1225.

Roddier, F. (1999). *Adaptive optics in astronomy*, Cambridge university press, Cambridge, United Kingdom.

Sarazin, M. (1990). The ESO differential image motion monitor. *Astron. Astrophys.*, Vol. 227: 294–300.

Shack, R. V. & Platt, B. C. (1971). Production and use of a lenticular Hartmann screen, *J. Opt. Soc. Am.*, Vol. 61: 656.

Southwell, W. H. (1980). Wavefront estimation from wavefront slope measurements, *J. Opt. Soc. Am.*, Vol. 70(8): 998–1006.

Tay, C. G.; Quan, C.; Fu, Y. & Huang, Y. (2004). Instantaneous velocity, displacement, and contour measurement by use of shadow moiré and temporal wavelet analysis, *Appl. Opt.*, Vol. 43: 4164–4171.

Ziad, A.; Conan, R.; Tokovinin, A.; Martin, F. & Borgnino, J. (2000). From the grating scale monitor to the generalized seeing monitor, *Appl. Opt.*, Vol. 39: 5415–5425.

Walker, C. A. (2004). *Handbook of moiré measurement*, Institute of Physics, London.

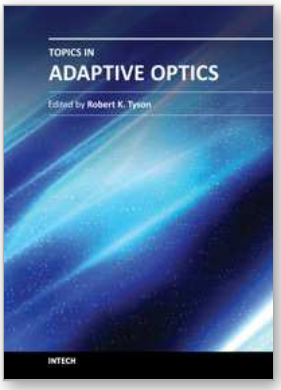


**Topics in Adaptive Optics**
Edited by Dr. Bob Tyson

ISBN 978-953-307-949-3
Hard cover, 254 pages
**Publisher** InTech
**Published online** 20, January, 2012
**Published in print edition** January, 2012

Advances in adaptive optics technology and applications move forward at a rapid pace. The basic idea of wavefront compensation in real-time has been around since the mid 1970s. The first widely used application of adaptive optics was for compensating atmospheric turbulence effects in astronomical imaging and laser beam propagation. While some topics have been researched and reported for years, even decades, new applications and advances in the supporting technologies occur almost daily. This book brings together 11 original chapters related to adaptive optics, written by an international group of invited authors. Topics include atmospheric turbulence characterization, astronomy with large telescopes, image post-processing, high power laser distortion compensation, adaptive optics and the human eye, wavefront sensors, and deformable mirrors.

**How to reference**
In order to correctly reference this scholarly work, feel free to copy and paste the following:

Saifollah Rasouli (2012). Atmospheric Turbulence Characterization and Wavefront Sensing by Means of the Moiré Deflectometry, Topics in Adaptive Optics, Dr. Bob Tyson (Ed.), ISBN: 978-953-307-949-3, InTech, Available from: http://www.intechopen.com/books/topics-in-adaptive-optics/atmospheric-turbulence-characterization-and-wavefront-sensing-by-means-of-the-moir-deflectometry

INTECH
open science | open minds

**InTech Europe**
University Campus STeP Ri
Slavka Krautzeka 83/A
51000 Rijeka, Croatia
Phone: +385 (51) 770 447
Fax: +385 (51) 686 166
www.intechopen.com

**InTech China**
Unit 405, Office Block, Hotel Equatorial Shanghai
No.65, Yan An Road (West), Shanghai, 200040, China
中国上海市延安西路65号上海国际贵都大饭店办公楼405单元
Phone: +86-21-62489820
Fax: +86-21-62489821